Minimal Model for Intracellular Calcium Oscillations and Electrical Bursting in Melanotrope Cells of *Xenopus Laevis*

L. Niels Cornelisse
Department of Cellular Animal Physiology and Department of Biophysics, Nijmegen Institute for Neurosciences, University of Nijmegen, 6525 ED Nijmegen, The Netherlands

Wim J. J. M. Scheenen
Werner J. H. Koopman
Eric W. Roubos
Department of Cellular Animal Physiology, Nijmegen Institute for Neurosciences, University of Nijmegen, 6525 E Nijmegen, The Netherlands

Stan C. A. M. Gielen
Department of Biophysics, Nijmegen Institute for Neurosciences, University of Nijmegen, 6525 EZ Nijmegen, The Netherlands

A minimal model is presented to explain changes in frequency, shape, and amplitude of Ca^{2+} oscillations in the neuroendocrine melanotrope cell of *Xenopus Laevis*. It describes the cell as a plasma membrane oscillator with influx of extracellular Ca^{2+} via voltage-gated Ca^{2+} channels in the plasma membrane. The Ca^{2+} oscillations in the *Xenopus* melanotrope show specific features that cannot be explained by previous models for electrically bursting cells using one set of parameters. The model assumes a K_{Ca}-channel with slow Ca^{2+}-dependent gating kinetics that initiates and terminates the bursts. The slow kinetics of this channel cause an activation of the K_{Ca}-channel with a phase shift relative to the intracellular Ca^{2+} concentration. The phase shift, together with the presence of a Na^{+} channel that has a lower threshold than the Ca^{2+} channel, generate the characteristic features of the Ca^{2+} oscillations in the *Xenopus* melanotrope cell.

1 Introduction

Cells of multicellular organisms communicate with each other to control and coordinate their activities. This communication takes place by way of various types of first messengers, such as neurotransmitters, hormones, and growth factors. First messengers specifically contact a cell via receptors that subsequently transduce the extracellular signals into specific (intra-) cellular responses such as protein synthesis, secretion, or contraction. In this transduction process, a relatively small number of second-messenger molecules

are involved, such as cAMP, inositol trisphosphate, and Ca^{2+} ions. Among the second messengers, to date much attention is being paid to the role of the intracellular Ca^{2+} concentration ($[Ca^{2+}]_i$) (Berridge, 1998; Bito, 1998; Neher, 1998). In many secretory cells, including neurons and neuroendocrine cells, $[Ca^{2+}]_i$ changes in the form of Ca^{2+} oscillations are thought to control secretory events (Stojilkovic & Catt, 1992; Shibuya & Douglas, 1993; Berridge, 1998). In some cases these oscillations depend on the influx of extracellular Ca^{2+} via voltage-gated Ca^{2+} channels in the plasma membrane and on Ca^{2+} release from intracellular stores. In others, the influx of extracellular Ca^{2+} is the only cause of the Ca^{2+} oscillations (Stojilkovic & Catt, 1992; Scheenen, Jenks, Roubos, & Willems, 1994; Scheenen, Jenks, Willems, & Roubos, 1994; Stojilkovic, Tomic, Kukulijan, & Catt, 1994). In the latter cell type, the Ca^{2+} influx depends on the electrical state of the plasma membrane.

Several models have been proposed for the mechanism by which Ca^{2+} oscillations are coupled to bursting electrical membrane activity, such as for the pancreatic β-cell (Chay & Keizer, 1983) and the R15 neuron in *Aplysia* (Chay, 1990; Canavier, Clark, & Byrne, 1991). However, although these models describe the electrical behavior of the cells, relatively little attention has been paid to the characteristics of the Ca^{2+} oscillations. Recently, several interesting details have been reported on Ca^{2+} oscillations in the melanotrope cell of the amphibian *Xenopus Laevis* (Scheenen, Jenks, van Dinter, & Roubos, 1996; Koopman, Scheenen, Roubos, & Jenks, 1997; Lieste et al., 1998). This neuroendocrine cell type is located in the intermediate lobe of the pituitary gland and secretes α-melanophore-stimulating hormone (α-MSH), which stimulates the dispersion of the pigment melanin in dermal melanophores. This process enables the animal to adjust the gray intensity of its skin to the light intensity of the environment (background adaptation). The *Xenopus* melanotrope cell is an established and extensively studied object for investigations of the ways in which environmental stimuli are transduced into physiologically meaningful responses (Loh & Gainer, 1977; Maruthainar, Loh, & Smyth, 1992; Artero, Fasolo, Andreone, & Franzoni, 1994; Roubos, 1997; Jenks et al., 1998). Many of the various steps in this transduction process are known in great detail and can be experimentally approached and quantitatively manipulated both in vivo and in vitro. Various neuronal messengers, such as thyrotropin-releasing hormone (TRH), corticotropin-releasing hormone (CRH), acetylcholine, serotonin (all excitatory) and dopamine, neuropeptide Y (NPY), and γ -aminobutyric acid (GABA) (all inhibitory) control the secretion of α-MSH from the *Xenopus* melanotrope cells (for reviews see Roubos, 1997; Jenks et al., 1998). All of these factors exert their effect on α-MSH secretion by affecting the Ca^{2+} oscillatory dynamics (Shibuya & Douglas, 1993; Scheenen, Jenks, Roubos, & Willems, 1994; Scheenen, Jenks, Willems, & Roubos, 1994). Recently, we showed that the Ca^{2+} oscillations are coupled to membrane action potential bursting (Lieste et al., 1998). Imaging of the $[Ca^{2+}]_i$ oscillations with high temporal resolution has revealed that the oscillation patterns may differ in

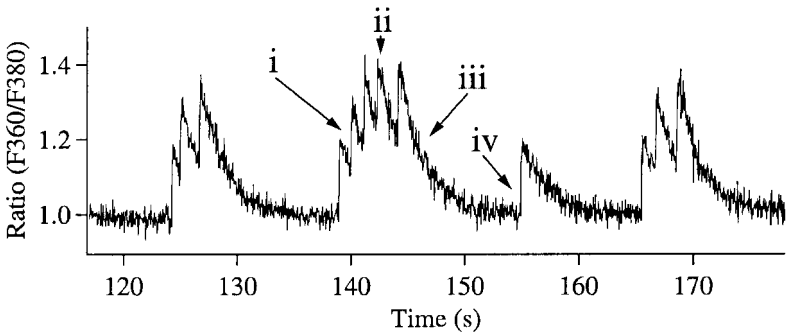

Figure 1: Characteristic features of Ca^{2+} oscillations in the *Xenopus* melanotrope cell: (i) steps during the rise phase, (ii) plateau phase, (iii) exponential decline phase, (iv) abrupt transition from decline to rise phase. The cell has been loaded with the membrane permeable probe fura-2/AM and fluorescence emission was monitored at 520 nm (SD 15 nm; described in Lieste et al., 1998). Changes in $[Ca^{2+}]_i$ are expressed as ratio signals of fura-2 fluorescence after excitation at 360 nm and 380 nm (F360/F380).

frequency, amplitude, and shape. In more detail, the Ca^{2+} oscillatory pattern of this cell is characterized by various other features such as (i) repetitive steps during the rise phase, (ii) a plateau phase, (iii) an exponential decline, and (iv) an abrupt transition from the decline phase to the rise phase of the next Ca^{2+} peak (Scheenen et al., 1996; Koopman et al., 1997; Lieste et al., 1998), as illustrated in Figure 1.

The aim of this study is to develop a mathematical model that describes the detailed features of Ca^{2+} oscillations in the *Xenopus* melanotrope cell and links these features to the electrical behavior of its plasma membrane. For this purpose we have taken the Chay-Rinzel model (Chay & Rinzel, 1985) as a starting point. This model provides a qualitative description of Ca^{2+} oscillations with steps in the rise phase as a result of the coupling between bursting electrical membrane activity and $[Ca^{2+}]_i$. However, it cannot explain properties (ii)–(iv) of the *Xenopus* melanotrope as described above. Therefore, we have replaced in the model the original Ca^{2+}-sensitive K^+-channel by a K_{Ca}-channel with Hodgkin-Huxley kinetics that are Ca^{2+} dependent and are slow compared to the kinetics of the voltage-gated channels. Furthermore, we have added an Na^+ channel that has a lower threshold than the Ca^{2+} channel. These modifications enable us to describe Ca^{2+} oscillations with the features that are characteristic for the melanotrope cell of *Xenopus Laevis*, as depicted in Figure 1. Whereas the model describes and explains the characteristics of the Ca^{2+} oscillations and the relationship between electrical membrane activity and Ca^{2+} oscillations in this neuroendocrine cell, it also provides insight into the physiological parameters of the

cell that can account for the variations in the pattern of the Ca^{2+} oscillations. This is highly relevant from a biological point of view, as it is assumed that variations in this pattern reflect different physiological states of this *Xenopus* neuroendocrine signal transducer cell (Koopman et al., 1997).

2 Model

2.1 Plasma Membrane Oscillator. In this section we describe the model to explain intracellular Ca^{2+} oscillations in the melanotrope cells of *Xenopus Laevis*. The model consists of a set of eight coupled, nonlinear differential equations and is based on a excitable membrane model proposed by Chay and Rinzel (1985). It contains a Hodgkin-Huxley-type formalism (Hodgkin & Huxley, 1952) for the generation of action potentials, a differential equation that describes the dynamics of $[Ca^{2+}]_i$, and a differential equation that describes the Ca^{2+}-dependent kinetics of a K_{Ca}-channel that provides the coupling between $[Ca^{2+}]_i$ and the electrical activity. Spontaneous Ca^{2+} action potentials are generated in a bursting manner. Each action potential gives rise to a rapid influx of Ca^{2+} through voltage-gated Ca^{2+} channels and causes a small increase in $[Ca^{2+}]_i$ (a "step") (Koopman et al., 1997). During a burst of action potentials, a number of steps are generated, which results in a sequential and accumulative increase in $[Ca^{2+}]_i$. In the time periods between the bursts of action potentials, Ca^{2+} is removed from the cell by a Ca^{2+} removal mechanism.

In the model, the fast kinetics of voltage-gated ion channels are combined with the slow kinetics of a K_{Ca}-channel that is progressively activated by an increase in $[Ca^{2+}]_i$. Activation (deactivation) of this slow K^+ channel causes a hyperpolarization (depolarization) of the plasma membrane. The activation and deactivation result in the stop and the start, respectively, of a burst of action potentials. On the basis of this concept for a plasma membrane oscillator, it is possible to describe the several characteristic features of the Ca^{2+} oscillations of the melanotrope cell, as given in the introduction.

2.2 Model Equations. The membrane potential (V) of an excitable cell is given by

$$C_m \frac{dV}{dt} = -\sum I_{ion} \tag{2.1}$$

where C_m represents the membrane capacitance, and $\sum I_{ion}$ the sum of the ion currents through the various ion channels. In this model the total ion current consists of five components:

$$\sum I_{ion} = I_{Ca,HH} + I_{Na,HH} + I_{K,HH} + I_L + I_{K,Ca}, \tag{2.2}$$

with the Hodgkin-Huxley type currents: $I_{Ca,HH}$, a voltage-gated Ca^{2+} current; $I_{Na,HH}$, a voltage-gated Na^+ current; $I_{K,HH}$, a voltage-gated K^+ current;

and I_L, a leak current, that incorporates the contributions of all the ion currents (e.g., Cl^- currents) not explicitly included in the model. The current $I_{K,Ca}$ represents a slow K^+ current that is activated by $[Ca^{2+}]_i$.

$I_{Ca,HH}$, $I_{Na,HH}$, $I_{K,HH}$, and I_L are modeled similarly to the ion currents in the original Hodgkin-Huxley scheme that describes the generation of action potentials (Hodgkin & Huxley, 1952). The currents are expressed in terms of a voltage-dependent conductance multiplied by the difference between the membrane voltage and the Nernst potential for the particular ion:

$$\begin{aligned} I_{Ca,HH} &= \bar{g}_{Ca,HH} m^3 h (V - V_{Ca}) \\ I_{Na,HH} &= \bar{g}_{Na,HH} p^3 q (V - V_{Na}) \\ I_{K,HH} &= \bar{g}_{K,HH} n^4 (V - V_K) \\ I_L &= \bar{g}_L (V - V_L), \end{aligned} \tag{2.3}$$

where $\bar{g}_{Ca,HH}$, $\bar{g}_{Na,HH}$, $\bar{g}_{K,HH}$, and $\bar{g}_L$ are the maximal conductances per unit area for the voltage-gated Ca^{2+}, voltage-gated Na^+, voltage-gated K^+, and leak channels, respectively. The symbols m, h, p, q, and n represent the probabilities to be in an open state for the m-, h-, p-, q-, and n-gates, respectively. V_{Ca}, V_{Na}, V_K, and V_L are the Nernst potentials for Ca^{2+}, Na^+, K^+, and leak ions, respectively, which are assumed to be constant in this study.

The time evolution of the probabilities m, h, p, q, and n is described by the following first-order differential equation, introduced by Hodgkin and Huxley:

$$\frac{dy}{dt} = \alpha_y (1 - y) - \beta_y y, \tag{2.4}$$

where y stands for m, h, p, q, or n and α_y and β_y are the activation and deactivation rates, respectively. The voltage dependencies of α_y and β_y have qualitatively the same form as in the original Hodgkin-Huxley equations, but are shifted along the V-axis in accordance with the Chay-Rinzel model. These shifts of the voltage dependencies of α_y and β_y result in the periodic generation of action potentials by the membrane. (The detailed expressions for α_y and β_y, used in this study are given in Table 2.)

The spontaneous activity of the membrane, as described above, can be blocked by a hyperpolarizing current. Alternating activation and deactivation of this current will generate bursts of action potentials. In this model, a slow potassium current, $I_{K,Ca}$, which is activated by Ca^{2+}, plays the role of the hyperpolarizing current. $I_{K,Ca}$ is given by

$$I_{K,Ca} = \bar{g}_{K,Ca} P (V - V_K), \tag{2.5}$$

where $\bar{g}_{K,Ca}$ is the maximal conductance per unit area for K_{Ca}-channel, P is the probability for the channel to be in an open state, and V_K is the Nernst

potential for K^+. The time evolution of P depends on $[Ca^{2+}]_i$ and is modeled by

$$\frac{dP}{dt} = \alpha_P(1 - P) - \beta_P P, \tag{2.6}$$

with α_P and β_P being the activation and deactivation rate, respectively. Equation 2.6 is analogous to equation 2.4. However, the rates in equation 2.6 are not voltage-dependent but are described by

$$\begin{aligned} \alpha_P &= u_o \left([Ca^{2+}]_i - [Ca^{2+}]_{basal} \right) \\ \beta_P &= u_c, \end{aligned} \tag{2.7}$$

with u_o and u_c constants, and $[Ca^{2+}]_{basal}$ the basal level of $[Ca^{2+}]_i$. The parameters u_o and u_c determine how P responds to an oscillating $[Ca^{2+}]_i$ signal. If both parameters are large relative to the rate of change of $[Ca^{2+}]_i$, P will closely follow changes in $[Ca^{2+}]_i$ and therefore will be almost in phase with $[Ca^{2+}]_i$. If the values of u_o and u_c are small relative to the rate of change of $[Ca^{2+}]_i$, P will lag changes in $[Ca^{2+}]_i$ and will be out of phase with respect to $[Ca^{2+}]_i$ for periodic changes in $[Ca^{2+}]_i$. Note that for large values of u_o and u_c the probability P for the K_{Ca}-channel to be in an open state can be replaced by its value at equilibrium,

$$P_\infty = \frac{\alpha_P}{\alpha_P + \beta_P} = \frac{\left([Ca^{2+}]_i - [Ca^{2+}]_{basal} \right)}{\left([Ca^{2+}]_i - [Ca^{2+}]_{basal} \right) + \frac{u_c}{u_o}}, \tag{2.8}$$

which, for $[Ca^{2+}]_{basal} = 0$, is the expression that was used by Chay and Rinzel (1985) for the open probability for the K_{Ca}-channel in their model.

The change in $[Ca^{2+}]_i$ depends on the influx of Ca^{2+} through the Ca^{2+} channels during an action potential and on the removal of free Ca^{2+} from the cytoplasm. Various mechanisms can be responsible for this removal, like a plasma-membrane-bound Ca^{2+}-ATPase that pumps Ca^{2+} out of the cell, mitochondrial uptake, and other fixed or mobile Ca^{2+} binding sites. Because the precise mechanisms underlying the efflux of Ca^{2+} in the melanotrope cell are unknown, the removal mechanism is modeled as simply as possible, by a linear flow proportional to $k_{Ca}([Ca^{2+}]_i - [Ca^{2+}]_{basal})$ with k_{Ca} the rate constant for the removal of Ca^{2+}. The equation that describes the change of free Ca^{2+} in the cytoplasm is therefore given by

$$\frac{d[Ca^{2+}]_i}{dt} = f \left\{ -\frac{3}{2rF} I_{Ca,HH} - k_{Ca} \left([Ca^{2+}]_i - [Ca^{2+}]_{basal} \right) \right\}, \tag{2.9}$$

where the term $-3/(2rF)$ reflects the scale factor to go from current per unit area to ion concentration for an ion with a double valence. This scale factor

is calculated by taking the ratio of the cell surface area to the cell volume, with r the radius of the cell, and by dividing it by the Faraday constant F and by a factor of two because of the double valence of Ca^{2+}. The parameter f determines how fast $[Ca^{2+}]_i$ changes in time and is defined by

$$f = \frac{d[Ca^{2+}]_i}{d[Ca^{2+}]_T}, \tag{2.10}$$

with $[Ca^{2+}]_T$ the total Ca^{2+} concentration inside the cell, i.e., the bound-plus-free cytosolic Ca^{2+} concentration (excluding $[Ca^{2+}]$ in stores) (Chay, 1990). In the case of fast buffering (faster than a millisecond), the inverse of parameter f can be expressed by

$$\begin{aligned} f^{-1} &= 1 + \frac{[B]}{K_B} \frac{1}{\left(1 + \frac{[Ca^{2+}]_i}{K_B}\right)^2} \\ &\approx 1 + \frac{[B]}{K_B} \end{aligned} \tag{2.11}$$

where $[B]$ represents the buffer concentration and K_B its dissociation constant (Chay, 1990). The second part of equation 2.11 is valid only if $K_B \gg [Ca^{2+}]_i$.

The set of eight coupled differential equations described in equations 2.1, 2.4, 2.6, and 2.9 was solved numerically, using the "lsode" method of the mathematical software MapleV release 5, by Waterloo Maple Inc., except for Figures 3 through 5, where we used the fourth-order Runge-Kutta method in a program written in C++ code.

3 Results

Figure 2 shows the response characteristics of the model as a function of time for $[Ca^{2+}]_i$ (see Figure 2A), the membrane potential V (see Figure 2B), and the fraction P of open K_{Ca}-channels (see Figure 2C). Figures 2A and 2B provide a clear illustration of the coupling between the membrane potential and the Ca^{2+} oscillations. The specific features of the Ca^{2+} oscillations in the *Xenopus* melanotrope cell, as given in Figure 1, are present in this simulation: steps in the rise phase of the Ca^{2+} peak (1), a plateau phase (2), an exponential decline phase (3), and an abrupt transition from the decline phase to the rise phase (4). Figure 2A also shows the increase in Ca^{2+} removal between the steps during the rise phase. The values for the parameters used in the simulations are listed in Table 1. In the following, we will discuss these features in more detail.

3.1 Coupling of $[Ca^{2+}]_i$ and Membrane Potential. Within each burst, the action potentials appear with a progressively increasing time interval.

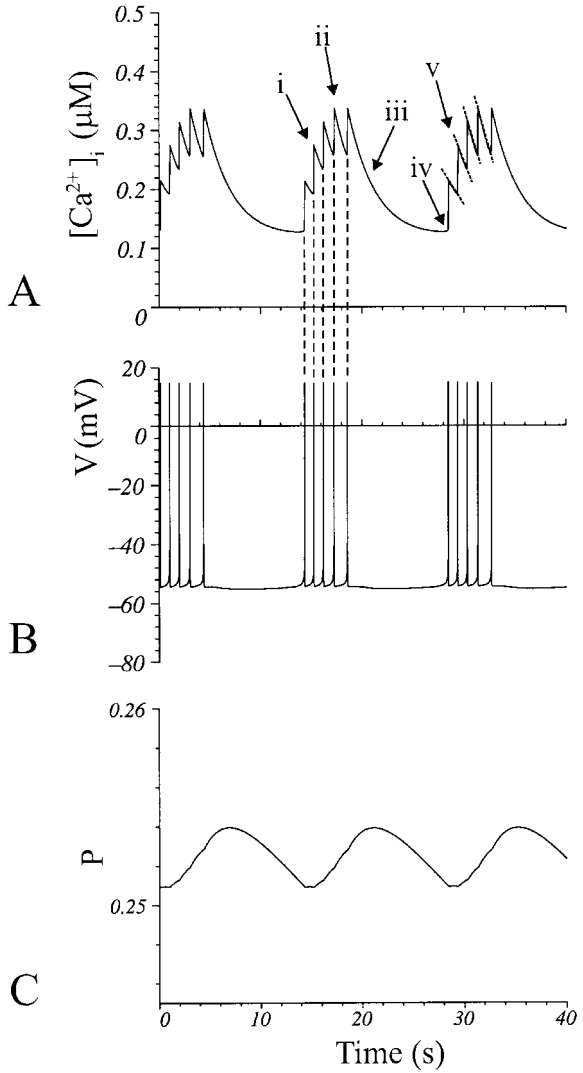

Figure 2: Simulation of spontaneous Ca^{2+} oscillations coupled to electrical bursting in the *Xenopus* melanotrope cell. In the calculated Ca^{2+} signal, the characteristic features of the Ca^{2+} oscillations in the *Xenopus* melanotrope cell are present: (i) steps in the rise phase, (ii) plateau phase, (iii) exponential decline, (iv) abrupt transition, (v) upregulation of Ca^{2+} removal, (vi) coupling between the plasma membrane action potentials, and the Ca^{2+} steps (A). Corresponding burst of action potentials (B). Fraction of open K_{Ca}-channels (C).

Table 1: Parameter Values.

C_m	=	$1\ \mu\text{F/cm}^2$
$\bar{g}_{\text{Ca,HH}}$	=	$2600\ \mu\text{S/cm}^2$
$\bar{g}_{\text{Na,HH}}$	=	$780\ \mu\text{S/cm}^2$
$\bar{g}_{\text{K,HH}}$	=	$2400\ \mu\text{S/cm}^2$
$\bar{g}_{\text{L}}$	=	$9.98\ \mu\text{S/cm}^2$
$\bar{g}_{\text{K,Ca}}$	=	$18\ \mu\text{S/cm}^2$
V_{Ca}	=	100 mV
V_{Na}	=	60 mV
V_{K}	=	−75 mV
V_{L}	=	−50.95 mV
V'	=	50 mV
V^n	=	30 mV
V^p	=	60 mV
V^q	=	55 mV
r	=	$8.9\ \mu\text{m}$
f	=	0.064
T	=	17°C
F	=	$9.65 \cdot 10^4$ C/mol
k_{Ca}	=	$6.2\ \text{s}^{-1}$
u_o	=	$0.01\ (\mu\text{M} \cdot \text{s})^{-1}$
u_c	=	$0.003\ \text{s}^{-1}$
V_0	=	−52 mV
P_0	=	0.251
$[Ca^{2+}]_{i,0}$	=	$0.13\ \mu\text{M}$
$[Ca^{2+}]_{basal}$	=	$0.1\ \mu\text{M}$ (in Figures 1 to 2 and 5 to 9)
$[Ca^{2+}]_{basal}$	=	$0\ \mu\text{M}$ (in Figures 3 to 5)

The sequence of action potentials is due to the combined effect of the voltage-dependent Ca^{2+}, Na^+, K^+, and leak channels. Each action potential causes a transient Ca^{2+} influx, as described by the first term at the right-hand side of equation 2.9. The second term at the right-hand side of equation 2.9 describes the removal of Ca^{2+}, which is proportional to $[Ca^{2+}]_i$. The sequential accumulation of Ca^{2+} ions in the cell causes an increase in $[Ca^{2+}]_i$. After several step increments, the mean $[Ca^{2+}]_i$ reaches a plateau due to the balance between the influx and the removal of Ca^{2+}. This is caused by the fact that Ca^{2+} removal is proportional to $[Ca^{2+}]_i$ and by the increase of the interval between subsequent action potentials. Once the generation of action potentials is stopped, there is no influx of Ca^{2+} anymore, and only

Table 2: Expressions for Activation (α) and Deactivation (β) rates for Probabilities n, m, h, p, and q, Characterizing the Dynamics of the Various Ion Channels.

$\alpha_n = \phi 2 \frac{(-(V+V^n)+10)}{e^{\frac{-(V+V^n)+10}{10}}-1}$,	$\beta_n = \phi 25 e^{\frac{-(V+V^n)}{80}}$
$\alpha_m = \phi 20 \frac{(-(V+V')+25)}{e^{\frac{-(V+V')+25}{10}}-1}$,	$\beta_m = \phi 800 e^{\frac{-(V+V')}{18}}$
$\alpha_h = \phi 14 e^{\frac{-(V+V')}{20}}$,	$\beta_h = \phi \frac{200}{e^{\frac{-(V+V')+30}{10}}+1}$
$\alpha_p = \phi 20 \frac{(-(V+V^p)+25)}{e^{\frac{-(V+V^p)+25}{10}}-1}$,	$\beta_p = \phi 800 e^{\frac{-(V+V^p)}{18}}$
$\alpha_q = \phi 14 e^{\frac{-(V+V^q)}{20}}$,	$\beta_q = \phi \frac{200}{e^{\frac{-(V+V^q)+30}{10}}+1}$

$\phi = 3^{(T-6.3)/10}$. See Table 1 for parameter values.

the right-hand term in equation 2.9 is different from zero, resulting in an exponential decline of $[Ca^{2+}]_i$.

The K_{Ca}-channels in our model are progressively activated by the buildup of $[Ca^{2+}]_i$ (see equation 2.6 and Figure 2C). The activated K_{Ca}-channels cause a hyperpolarization of the plasma membrane. This results in an increase in the time interval between the action potentials and finally stops the spontaneous generation of action potentials. In the resulting silent period of membrane activity, $[Ca^{2+}]_i$ decreases. As a result of this decrease, the fraction of activated K_{Ca}-channels P, which lags $[Ca^{2+}]_i$, decreases. This eventually leads to depolarization of the membrane, and action potential bursting is resumed. Thus, the periodic suppression of the spontaneous generation of action potentials as a result of the alternating activation and deactivation of the K_{Ca}-channels causes the bursting behavior of the membrane and the resulting $[Ca^{2+}]_i$ oscillations.

3.2 Dynamic Analysis of Models. In order to obtain insight into the qualitative properties of our model and to make a comparison between the properties of our model and the properties of the Chay-Rinzel model, we have applied a fast-slow analysis of the various dynamic features of the model. The main difference between our model and the Chay-Rinzel model refers to the parameter for the slow process, which controls the bursting. In the Chay-Rinzel model, the slow parameter is $[Ca^{2+}]_i$, which is directly coupled to electrical membrane activity. The dashed line in the phase-plane plot in Figure 3A shows the steady states of the fast subsystem of the Chay-Rinzel model for fixed values of the control parameter $[Ca^{2+}]_i$. This curve has three branches, where the upper and lower branches represent the stable states.

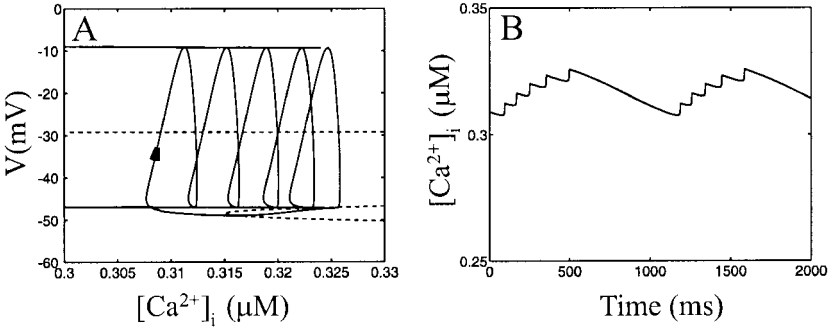

Figure 3: Fast-slow analysis for the Chay-Rinzel model: trajectory (solid line), periodic branches (heavy lines), and steady states (dashed curve) in the $[Ca^{2+}]_i$-V phase plane (A), Ca^{2+} oscillations in a small range above basal level (B). For further explanation, see text.

The upper branch denotes the regime for stable oscillatory states (limit cycles). The maximum and minimum values for the membrane potential in this regime are denoted by the heavy lines. The middle branch represents the unstable states, and the lower branch represents the stable steady state. Bursting occurs when the fast subsystem jumps between the two stable states. The transitions are controlled by the slow parameter $[Ca^{2+}]_i$. During the active phase of the Chay-Rinzel model, there is an influx of Ca^{2+}, and the cycles, corresponding to action potentials, continue. As a consequence, $[Ca^{2+}]_i$ increases until the system crosses the middle branch representing the unstable states. Then the limit cycle behavior stops, and the system will show a relaxation to the lower branch. Meanwhile $[Ca^{2+}]_i$ decreases until the system leaves the lower branch and jumps to the upper branch, which initiates a new sequence of action potentials. This type of behavior has been classified as *square bursting* (Wang & Rinzel, 1995). Note that the changes in $[Ca^{2+}]_i$ (see Figure 3B) lack an exponential decline phase that returns to basal level and a plateau phase, phases that are characteristic for the activity of the melanotrope cell.

In our model, we are dealing with two slow parameters. The first is parameter P, which is the slow parameter that controls the bursting; it depends on the second slow parameter $[Ca^{2+}]_i$, which is again coupled to the electrical membrane activity. The 3D plot in Figure 4A reveals the relation between membrane potential V, $[Ca^{2+}]_i$, and P. Figure 4B shows the projection on the P-V plane. As in Figure 3A, the dashed curve represents the stable and unstable steady states. Importantly, the trajectory in the P-V plane differs from the trajectory in Figure 3A. In Figure 3A, $[Ca^{2+}]_i$ decreases between two action potentials, whereas in Figure 4B the slow parameter P increases steadily during the sequence of action potentials. Figure 4C, which gives the

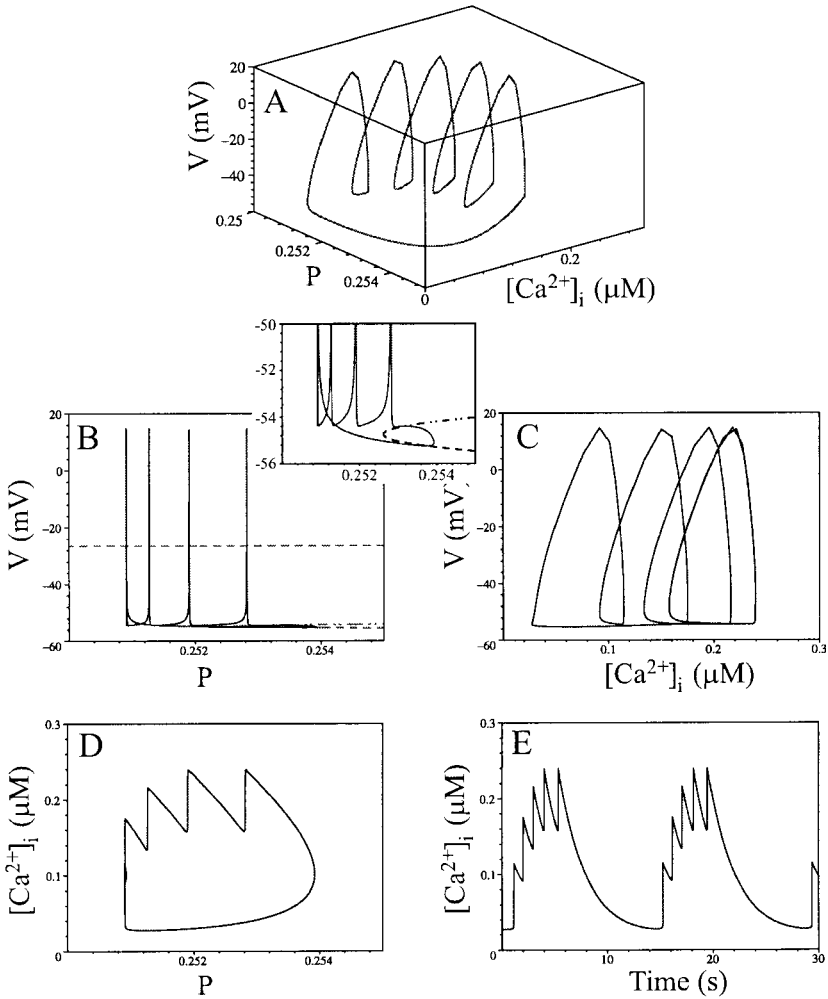

Figure 4: Fast-slow subsytem analysis of our model. (A) 3D-plot of trajectory in P-$[Ca^{2+}]_i$-V phase space. (B) Projection of the trajectory (solid line) and steady states for different values of P (dashed curve) in the P-V plane. (C) Projection in the $[Ca^{2+}]_i$-V plane. (D) Projection in the P-$[Ca^{2+}]_i$ plane. (E) Simulated Ca^{2+} oscillations.

relation between V and $[Ca^{2+}]_i$, is qualitatively similar for the Chay-Rinzel model and our model. However, in Figure 4C, the cycles tend to approximate a limit cycle in the $[Ca^{2+}]_i$-V plane. This limit cycle behavior in the $[Ca^{2+}]_i$-V plane corresponds to the plateau phase (see Figure 4E), where

the parameter P increases (see Figure 4D) until the trajectory in the P-V plane crosses the line with unstable steady states, which ends the oscillating pattern of action potentials. When the burst of action potentials stops, $[Ca^{2+}]_i$ decreases exponentially according to equation 2.9. After the burst of action potentials, parameter P continues for some time to increase due to the slow dynamics (see equation 2.6). After some time P starts to decrease (see Figure 4D) until the action potentials start again.

3.3 The Na^+ Channel. In our model the Na^+ channel is responsible for the depolarization that leads to the abrupt transition of the $[Ca^{2+}]_i$ signal from the decline to the rise phase. It opens at a membrane potential that is about 10 mV below that of the Ca^{2+} channel. Such a lower threshold is in agreement with experimental data (J. R. Lieste, unpublished data) and is implemented by a 10 mV larger voltage shift V^p for the activation variable p of the Na^+ channel compared to the voltage shift V' for the activation variable m for the Ca^{2+} channel. When the membrane is hyperpolarized after a burst of action potentials, the Na^+ current together with the leak current starts to depolarize the membrane very slowly. As a result of the slow depolarization of the membrane, the Na^+ current starts to increase slowly, while the Ca^{2+} current remains almost zero due to a higher threshold of the Ca^{2+} channels. At a certain point (near -54 mV) the Na^+ current starts to increase more rapidly and thereby initiates a rapid depolarization. Once the depolarization reaches the threshold for the Ca^{2+} channels, the Ca^{2+} current is activated rapidly, resulting in a sharp increase in $[Ca^{2+}]_i$.

Without the Na^+ channel, the small depolarizing current at the onset of a new burst would be generated by the Ca^{2+} channel. In the case that the decline phase reaches such low levels that the efflux proportional to $[Ca^{2+}]_i$ becomes very small, the Ca^{2+} influx due to this depolarizing current may exceed the efflux. This becomes evident as a smooth rising of $[Ca^{2+}]_i$ resulting in a smooth transition. Because the Chay-Rinzel model does not display exponential declines that come close to the basal level for $[Ca^{2+}]$ (see Figure 3B), the problem of abrupt transitions does not apply. Therefore, we compare our model with a minimal model for square-wave bursting (Rinzel & Ermentrout, 1998), which displays smooth transitions. This model is qualitatively the same as the Chay-Rinzel model, but uses simpler kinetics for the fast subsystem. Like the Chay-Rinzel model, this model has a voltage-dependent Ca^{2+} current as an inward current. The different behavior at the transition from decline to rise phase between the Rinzel-Ermentrout model and our model is illustrated best by looking at the $[Ca^{2+}]_i$-I_{Ca} phase plane.

In Figure 5A we plot the trajectory of this model in the $[Ca^{2+}]_i$-I_{Ca} plane. In order to represent time in this graph we added circles at equidistant time steps on top of the traces in the plane. When $[Ca^{2+}]_i$ becomes small, the trajectory slows down, resulting in a higher density of circles. For small values of $[Ca^{2+}]_i$, the trajectory slowly increases its speed while $[Ca^{2+}]_i$ is increasing again. This results in a smooth transition from the decline to the

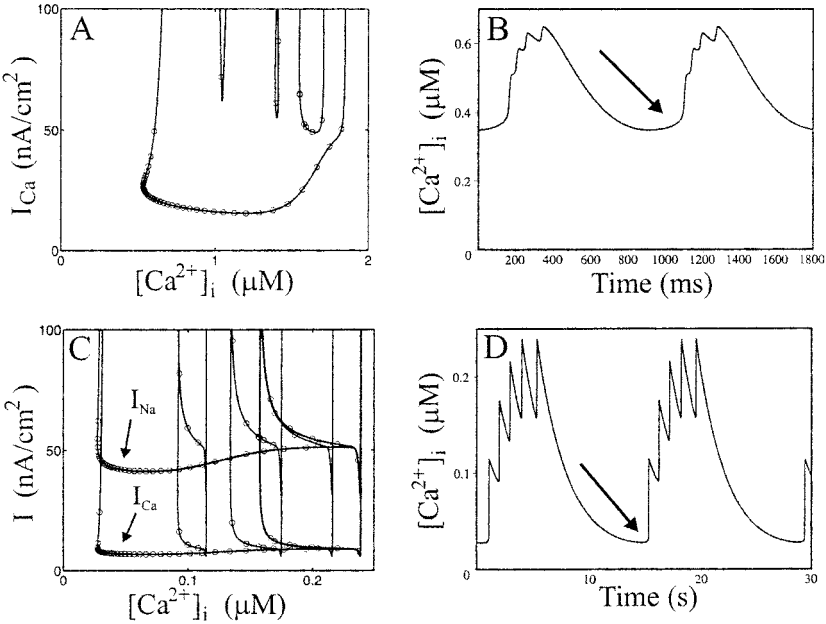

Figure 5: Trajectory of the Morris-Lecar model in the $[Ca^{2+}]_i$-I_{Ca} plane (A), resulting in a smooth transition from decline to rise phase for $[Ca^{2+}]_i$ (B). Trajectory for our model in the $[Ca^{2+}]_i$-I plane of I_{Ca} and I_{Na} (C), resulting in an abrupt transition from decline to rise phase for $[Ca^{2+}]_i$ (D). For both models the circles in the trajectories are plotted with time steps $\Delta t = 0.02\ T_p$. With T_p the period of one Ca^{2+} peak.

rise phase, as depicted in Figure 5B. For our model, both the trajectories for I_{Na} and I_{Ca} are plotted in the $[Ca^{2+}]_i$-I plane, with equidistant time steps, in Figure 5C. When $[Ca^{2+}]_i$ decreases, both trajectories slow down. At some point (near $[Ca^{2+}]_i = 0.05\,\mu$M) I_{Ca} remains fairly constant, while I_{Na} starts to increase slowly. Near $[Ca^{2+}]_i = 0.04\ \mu$M I_{Na} starts to increase rapidly. This is the start of a new action potential, which subsequently causes a rapid increase of I_{Ca}. This illustrates the abrupt transition from the decline to the rise phase, as shown in Figure 5D.

Recent experiments with combined measurements of action currents and $[Ca^{2+}]_i$ have revealed a blockage of electrical membrane activity of the cell and a return of $[Ca^{2+}]_i$ to basal level in Na^+-free medium (Na^+ replaced by N-methyl-D-glucamine; NMDG) (Lieste et al., 1998) (see also Figure 6A). Under these conditions, electrical activity can be induced again by applying a depolarizing 20 mM K^+ pulse extracellularly. This induced activity generates a large Ca^{2+} peak due to the continuous firing at a higher frequency

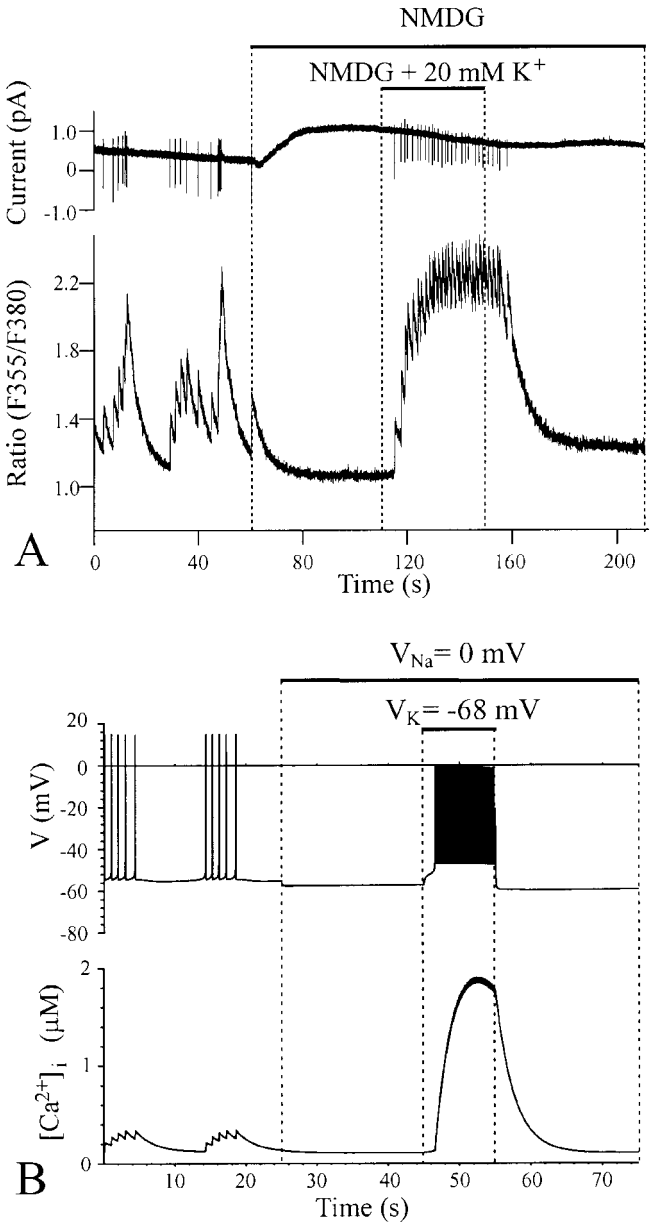

Figure 6: Effect of extracellular Na^+ with or without a depolarizing K^+ pulse, on the electrical activity of the plasma membrane and the $[Ca^{2+}]_i$ (after Lieste et al., 1998) (A). Simulation of the experiment in Figure 3A. The Na^+ removal is modeled by $V_{Na} = 0$ mV and the depolarizing K^+ pulse by $V_K = -68$ mV (B).

than under normal conditions. After returning to Na^+ free medium without 20 mM K^+, the membrane activity is blocked again, and $[Ca^{2+}]_i$ returns in an exponential way to its basal level.

This experiment can be simulated with our model, as illustrated in Figure 6B. In the simulation the removal of Na^+ is modeled by setting the Nernst potential for Na^+ to a value close to 0 mV. This is done because during the washout of the normal bathing solution with Na^+ free medium, the concentration of Na^+ is assumed to drop to very low values similar to the concentration of Na^+ inside the cell. This results in a blockage of the electrical activity and in a return of $[Ca^{2+}]_i$ to basal level. The effect of the depolarizing K^+-pulse is simulated by increasing the Nernst potential for K^+ from -75 mV to -68 mV. It can be observed that a 20 mM K^+ pulse leads to a larger shift in V_K than that performed in the simulation. However, recent experiments have confirmed that a less strong K^+ pulse of 5 mM is sufficient to induce a Ca^{2+} transient in silent cells similar to that of Figure 6A (Scheenen, personal communication). The membrane starts to generate action potentials again, with a high frequency, resulting in a large Ca^{2+} peak. Setting the V_K to -75 mV again, but leaving V_{Na} at 0 mV, stops the firing of action potentials and results in an exponential decline of $[Ca^{2+}]_i$ to the basal level.

3.4 Parameter Dependence of the Ca^{2+} Oscillations. Various parameters in our model affect the shape and frequency of the Ca^{2+} oscillations. In this section we will investigate the effect of four important parameters, u_o and u_c in equation 2.7, and k_{Ca} and f in equation 2.9, and to what extent these parameters can account for the variation of patterns in one cell and among different cells. In Figures 7 through 9 the $[Ca^{2+}]_i$ is shown in the first column (A). The corresponding graphs of the fraction of open K_{Ca}-channels P are shown in the second column (B), and the membrane potential V is given in the third column (C). All parameter settings are the same as in Figure 2, unless explicitly stated otherwise.

Figure 7 shows the results for different parameter values of u_o. Since the rate of active K_{Ca}-channels, dP/dt, is a function of both the positive term $u_o([Ca^{2+}]_i - [Ca^{2+}]_{basal})(1-P)$ and the negative term $-u_cP$ in the right-hand side of equation 2.6, increasing u_o will have the same effect qualitatively as decreasing u_c: an enhancement of the activation of the K_{Ca}-channel for the same levels of $[Ca^{2+}]_i$. Therefore, we will discuss the case only for u_o.

For slow activation ($u_o = 0.005$ $(\mu M\ s)^{-1}$), the simulated $[Ca^{2+}]_i$ shows a continuous sequence of Ca^{2+} steps, which, after some initial settling time, remains at a constant level above basal level. The mean level of $[Ca^{2+}]_i$ reached after about 20 steps reflects a balance between influx and removal of Ca^{2+} in equation 2.9. The corresponding electrical activity is a continuous firing of action potentials. After the initial settling, the fraction of open channels is constant, which implies a balance between activation and deactivation in equation 2.6. The product of u_o with the plateau level of $[Ca^{2+}]_i$ results

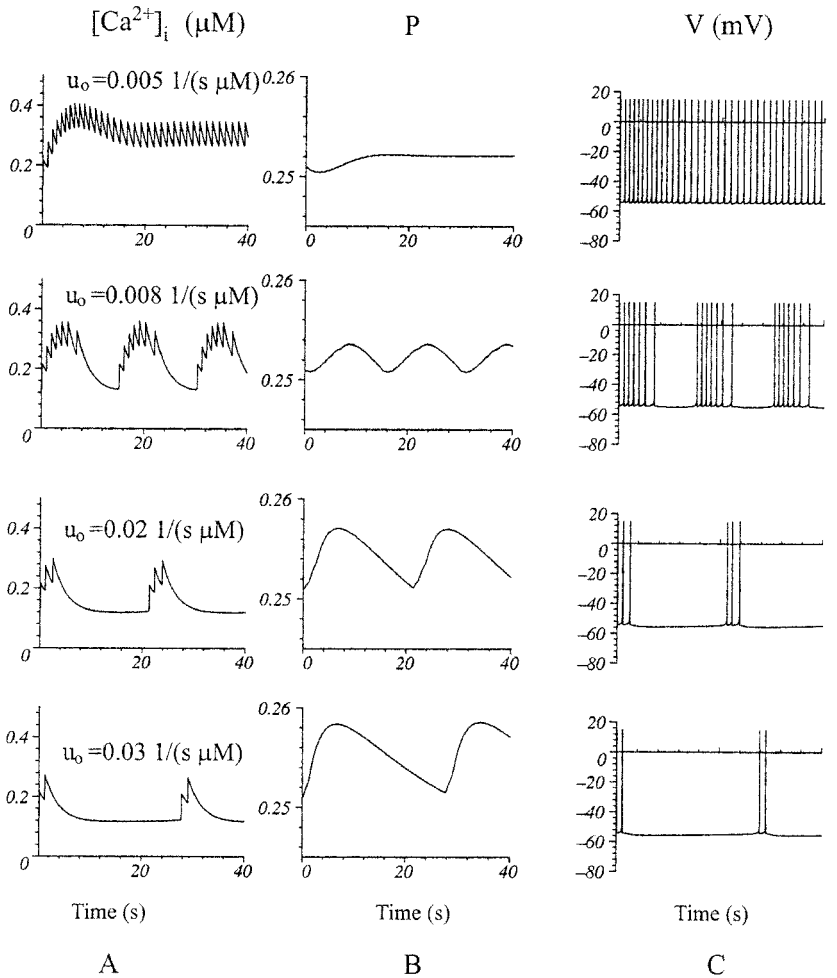

Figure 7: Results for different values of parameter u_o on the internal Ca^{2+} concentration (A), fraction of open K_{Ca}-channels (B), and the membrane potential (C).

in an activation of the K_{Ca}-channels that is large enough to decrease the frequency of the action potential firing but not large enough to stop membrane activity. For larger values of u_o ($u_o = 0.008$ $(\mu \mathrm{M\ s})^{-1}$ and higher) the activation of the K_{Ca}-channel is increased, which leads to hyperpolarization that is strong enough to end the burst of action potentials. This is necessary to obtain the bursting and oscillating behavior of the cell as described in the previous section. Increasing u_o also decreases the number of steps in a Ca^{2+}

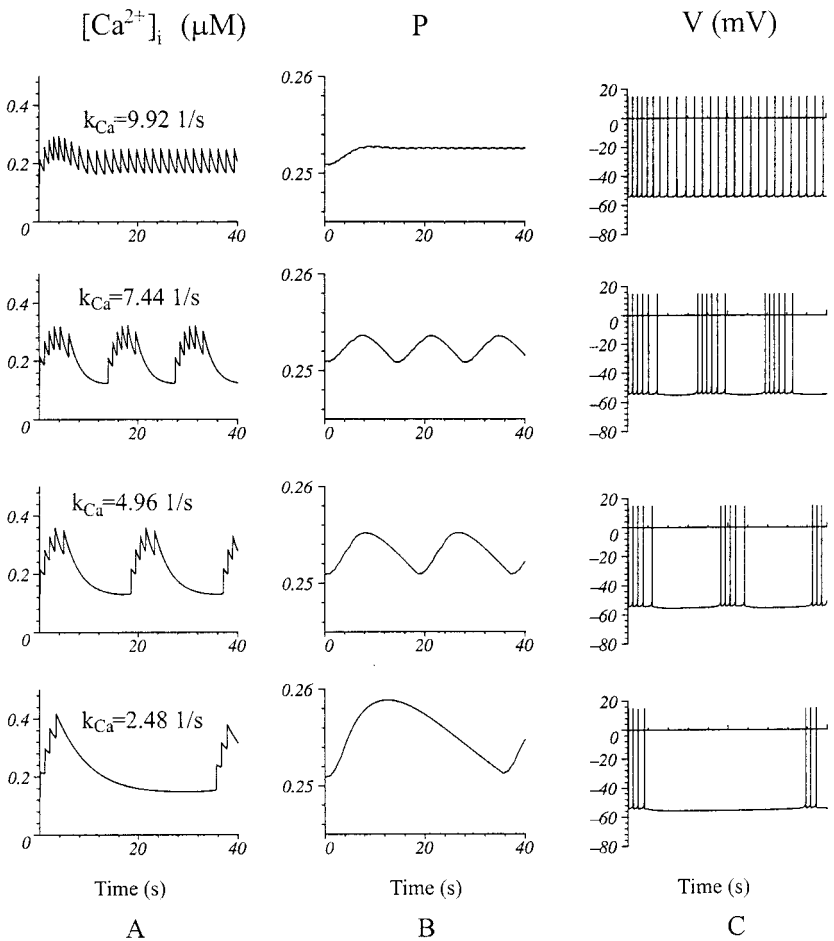

Figure 8: Results for different values of parameter k_{Ca} on the internal Ca^{2+} concentration (A), fraction of open K_{Ca}-channels (B), and the membrane potential (C).

peak and increases the length of the decline phase. The latter is related to a shorter burst and a longer interburst interval of the membrane potential.

The simulations for different removal rates k_{Ca} are shown in Figure 8. The upper panel of Figure 8 shows the $[Ca^{2+}]_i$ in the case of fast pumping of Ca^{2+} ($k_{Ca} = 9.92\ s^{-1}$). After an initial settling, it shows a continuous sequence of Ca^{2+} steps at a constant level above basal level. The pattern is very similar to the upper panel in Figure 7A, but the mean level of $[Ca^{2+}]_i$ is lower. This is due to the stronger removal compared to that in Figure 7,

which settles the balance between influx and efflux in equation 2.9 at a lower $[Ca^{2+}]_i$ level. The corresponding graph of the membrane potential (see Figure 8C) shows a continuous firing of action potentials. The fraction of activated K_{Ca}-channels is constant, and it is large enough to decrease the frequency of action potential firing but not large enough to stop membrane activity.

Decrease of the removal rate k_{Ca} results in a smaller value for the second term $k_{Ca}[Ca^{2+}]_i$ on the right-hand side of equation 2.9. The resulting smaller efflux allows a faster buildup of $[Ca^{2+}]_i$ during the rise phase and a slower decrease of $[Ca^{2+}]_i$ in the decline phase. This is reflected by a faster activation of the K_{Ca}-channel and a slower deactivation. As a consequence, the number of steps per peak and the frequency of the oscillations are reduced for smaller removal rates k_{Ca}. Moreover, the frequency of the Ca^{2+} oscillations is also decreased due to the higher levels of activation of the K_{Ca}-channels that are reached, which requires more time to deactivate them.

The results for different values for parameter f are shown in Figure 9. In the case of strong buffering (small f) the change of free Ca^{2+}, relative to the change of the total amount of Ca^{2+} in the cell, is small. Therefore, in this case, each action potential gives a small contribution to the buildup of the Ca^{2+} peak (see equation 2.9 and the upper panel of Figure 9). Due to this slow increase of $[Ca^{2+}]_i$ the activation of the K_{Ca}-channels is slow, which causes long bursts of action potentials. The fact that f is small in equation 2.9 also accounts for the slow decrease of free Ca^{2+}. This causes slow deactivation of the K_{Ca}-channels and therefore long interburst intervals. When the buffering becomes weaker (i.e., when f is increased; lower panels in Figure 9), the steps in the rise phase of the Ca^{2+} peaks increase, yielding a faster buildup of $[Ca^{2+}]_i$. This leads to faster activation of the K_{Ca}-channels, resulting in shorter bursts. Furthermore, faster deactivation, due to faster decrease of $[Ca^{2+}]_i$, yields shorter interburst intervals.

4 Discussion

We present a minimal model to explain the various characteristic features of Ca^{2+} oscillations and the electrical bursting of the neuroendocrine melanotrope cell in the pituitary gland of *Xenopus Laevis*. Two important aspects of the model are new compared to previous models for bursting cells. These aspects concern the relatively slow Ca^{2+}-dependent Hodgkin-Huxley kinetics for the Ca^{2+}-sensitive K^+-channel, and the action of the Na^+ channel. They are necessary to reveal the specific features of the Ca^{2+} oscillations as measured in the *Xenopus* melanotrope cell. These features are (1) steps (typical range 1 to 10) in the rise phase of a Ca^{2+} peak, (2) a plateau phase at the end of the rise phase, (3) an exponential decline, (4) an abrupt transition from decline to rise phase, (5) an increase in the removal rate of Ca^{2+} during the rise phase, and (6) the coupling between the plasma membrane action potentials and the Ca^{2+} steps.

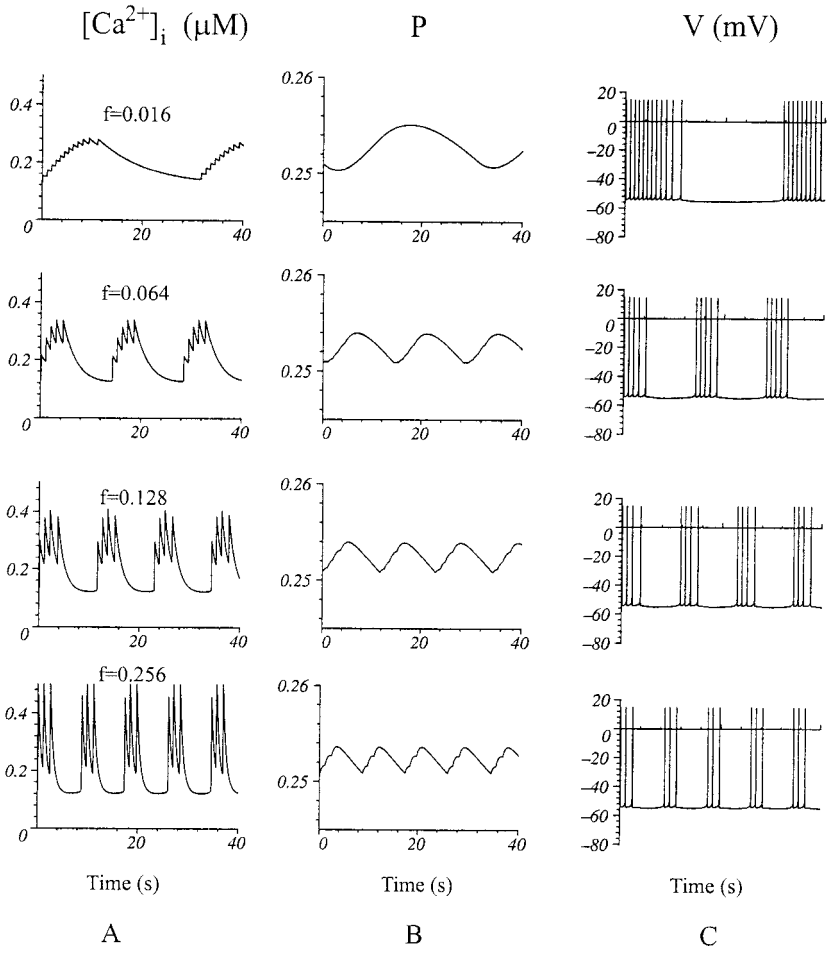

Figure 9: Results for different values of parameter f on the internal Ca^{2+} concentration (A), fraction of open K_{Ca}-channels (B), and the membrane potential (C).

Various models by Chay and Kreizer (1983), Chay and Rinzel (1985), Chay (1990, 1996), and Canavier et al. (1991) have been proposed to explain the electrical bursting activity of the plasma membrane coupled to oscillations of $[Ca^{2+}]_i$. These models describe the electrical behavior of the various bursting cell types but pay little attention to specific characteristics of the Ca^{2+} oscillations. They have in common that the ion channels that hyperpolarize (depolarize) the plasma membrane in order to terminate (initiate) bursts of action potentials are directly activated (inactivated) by $[Ca^{2+}]_i$. This implies that their activity is in phase with $[Ca^{2+}]_i$. As a consequence,

these models can only describe Ca^{2+} oscillations in a relatively small range above basal level, which is the level where the $[Ca^{2+}]_i$ will return to after blocking the electrical activity of the membrane (Canavier et al., 1991: 100 up to 200 nM above basal level with amplitude of 100 up to 200 nM; Chay, 1996: 500 nM above basal level with amplitude of 100 nM; and Chay and Rinzel, 1985: 300 nM above basal level with amplitude of 20 nM). The Ca^{2+} oscillations in the *Xenopus* melanotrope cell have amplitudes in the order of 300 nM (Shibuya & Douglas, 1993) and they return to basal level after each Ca^{2+} peak (Lieste et al., 1998).

In general, the buildup of a Ca^{2+} peak in the Chay and Canavier models is by a large number of steps corresponding to the number of action potentials in each burst. If the number of steps in the Ca^{2+} peaks is fewer than 10, the Ca^{2+} peaks show no plateaus. In the *Xenopus* melanotrope cell plateaus are generally observed after three to four steps. In the Chay and Canavier models, it is not possible to vary the length of the decline phase without changing the slope of the exponential decline. However, in the *Xenopus* melanotrope, there is a strong variability in the lengths of the decline phases of the Ca^{2+} peaks while the slopes can be described with the same exponential.

The model we propose here is based on the Chay-Rinzel model (1985), modified in such a way that it describes the specific features of the Ca^{2+} oscillations in the melanotrope cell. The assumptions in our model and the parameter dependence of the Ca^{2+} oscillations will be discussed in the next two sections.

4.1 Assumptions of the Model. *The K_{Ca}-channel*. We have replaced the K_{Ca}-channel in the Chay-Rinzel model by a K_{Ca}-channel that has Hodgkin-Huxley gating kinetics that are relatively slow with respect to the gating kinetics of the voltage-sensitive channels in the model. The activation process of the K_{Ca}-channel in our model is purely Ca^{2+}-dependent with a relatively long time constant, such that the channel activity lags the changes in $[Ca^{2+}]_i$, resulting in a phase shift between $[Ca^{2+}]_i$ and the slow K_{Ca}-channel activity. The proposed gating kinetics for the K_{Ca}-channel, which initiates and terminates the bursts of action potentials, lead to new results compared to the previous models for bursting cells by Chay and Rinzel (1985), Chay (1990, 1996) and Canavier et al. (1991): the model simulates Ca^{2+} peaks with a variable number of steps in the typical range of 1–10; the peaks start at basal level, approaching in some peaks, but not in all, a plateau level; and the $[Ca^{2+}]_i$ then returns exponentially to its basal level.

Various mechanisms can account for the slow kinetics of the K_{Ca}-channel. A possible candidate for this mechanism is Ca^{2+}-dependent phosphorylation of the channel as proposed by Goldbeter (1996). In this terminology P in equation 2.6 stands for the fraction of phosphorylated channels. The term $u_o([Ca^{2+}]_i - [Ca^{2+}]_{basal})$ is the Ca^{2+}-dependent conversion rate from the dephosphorylated state to the phosphorylated state, which is in fact the

activity of the protein kinase. Parameter u_c is the conversion rate from the phosphorylated state to the dephosphorylated state, or the activity of the phosphatase. There is ample evidence that some K_{Ca}-channels can be regulated in this way. For instance, the α-subunit of the BK channel ("Big K^+ channel") displays putative phosphorylation sites (Vergara, Latorre, Marrion, & Adelman, 1998). Furthermore, modulation of BK channels by phosphorylation is reported by Reinhart and Levitan (1995). They showed that the endogenous protein kinase activity is protein kinase C (PKC)-like. The increase in open probability due to phosphorylation occurs gradually over a period of minutes. This is in the same order of magnitude as the time constant for the channel kinetics of the K_{Ca}-channel in our model, which is given by $\tau_P = 1/(u_o([Ca^{2+}]_i - [Ca^{2+}]_{basal}) + u_c)$ and which is about 4 minutes. An explanation of the dynamics of the melanotrope cell required the introduction of the slow kinetics of the K_{Ca}-channel. The dynamics of this channel are roughly in agreement with the dynamics of phosphorylation. However, the simple first-order differential equations (equations 2.6 and 2.7) to model this process may seem somewhat unrealistic. Since detailed experimental data are lacking, this simple approximation was sufficient for the purpose of this study and for this developing model of the *Xenopus* melanotrope cell.

Na^+ channel. In the models of Chay and Rinzel (1985) and Canavier et al. (1991), which lack a Na^+ channel, the transitions from the decline to the rise phase are smooth for the Ca^{2+} oscillations that have an oscillation time of several seconds. The introduction in the model of a Na^+ channel, with a lower threshold than the Ca^{2+} channel, explains the abrupt transition from the decline to the rise phase, as measured in the melanotrope cell. Independent evidence for a role of Na^+ channels comes from experiments by Lieste et al. (1998), which have shown that removal of extracellular Na^+ eliminates the electrical activity of the plasma membrane and blocks the Ca^{2+} oscillations. As a result, the $[Ca^{2+}]_i$ returns to basal level. Restoration of the electrical activity can be obtained by applying a depolarizing K^+ pulse extracellularly adding KCl, resulting in a large Ca^{2+} peak. We are able to simulate this experiment with the model, whereas models that lack a Na^+ channel and are therefore insensitive to Na^+ removal cannot reproduce these experimental results.

Ca^{2+} stores. In the cytoplasm, various stores are present that bind and release Ca^{2+}, such as the endoplasmic reticulum and the mitochondria (Pozzan, Rizzuto, Volpe, & Meldolesi, 1994). Experiments in the *Xenopus* melanotrope cell where these Ca^{2+} stores were manipulated show only minor modulatory effects on the Ca^{2+} oscillations, suggesting that stores are not involved in the generation of Ca^{2+} oscillations (Scheenen et al., 1994a, 1994b; Koopman et al., 1997). Therefore, our minimal model does not incorporate these Ca^{2+} stores as a source of Ca^{2+}. In this sense, the cell can be considered as a plasma membrane oscillator because the Ca^{2+} oscillations are determined by the plasma membrane activity only.

Ca^{2+} dynamics. The assumption in the model of Ca^{2+} removal proportional to $[Ca^{2+}]_i$ via the term $k_{Ca}([Ca^{2+}]_i - [Ca^{2+}]_{basal})$ is in good agreement with the experimental observations (Lieste et al., 1998). It adequately describes both the exponential decline and the increasing removal rate during the rise phase of the Ca^{2+} peak. Because the cell is modeled as one compartment, the distribution of Ca^{2+} is assumed to be homogeneous throughout the cell and also during changes in $[Ca^{2+}]_i$ due to efflux and influx of Ca^{2+} across the membrane. This is a plausible assumption, considering that the time interval between two steps and the time needed for Ca^{2+} to travel from the membrane throughout the whole cell is on the order of a second (Scheenen et al., 1996). Therefore, the distribution of Ca^{2+} in the cell will homogenize between two Ca^{2+} steps, which follow each other by intervals of about 1 second.

In the model, the buffering of Ca^{2+} is incorporated in the parameter f as described in equation 2.11. The exact buffer parameters for the *Xenopus* melanotrope cell are not known. However, we assume that these are not significantly different from the standard values in other cell types (Nowycky & Pinter, 1993). Therefore, we assume an equilibrium coefficient K_B of 5 μM and a buffer concentration $[B]$ of 0.5 mM. This results in a value for f of nearly 0.01, which is close to the values used in our simulations.

4.2 Dependence of the Oscillation Pattern on u_o, u_c, k_{Ca}, and f. In our model four crucial parameters control the shape and frequency of the Ca^{2+} oscillations. Two of these, u_o and u_c, affect the length of the rise and the decline phase (and thus the frequency, amplitude and the number of steps in each Ca^{2+} peak) without changing the exponent of the decline phase. Decreasing (increasing) the removal rate k_{Ca} decreases (increases) the frequency, amplitude, number of steps per Ca^{2+} peak, and slope of the decline phase. The parameter f, which expresses the change of free Ca^{2+} with respect to the change in the total intracellular Ca^{2+} concentration, affects the frequency, number of steps per peak, and amplitude of both the Ca^{2+} step and the Ca^{2+} peak.

Summarizing, we have constructed a mathematical model that not only neatly simulates all characteristics of the Ca^{2+} oscillation pattern in the *Xenopus* melanotrope cell, but also provides the possibility of testing the effects of neuronal factors (first messengers, such as neurotransmitters and neuropeptides) on this pattern via the parameters u_o, u_c, and k_{Ca}. This approach is of biological relevance, as it is assumed that changes in the oscillation pattern reflect differential regulations by various known regulatory neurotransmitters and neuropeptides (e.g., NPY, dopamine, GABA, TRH, CRF, and acetylcholine) of various cellular key processes, such as gene expression, protein biosynthesis, and secretion. We expect that application and further development of our model will stimulate neurobiological research on the role of neuronal factors in the control of cellular secretory processes.

References

Artero, C., Fasolo, A., Andreone, C. & Franzoni, M. F. (1994). Multiple sources of the pituitary pars intermedia innervation in amphibians: A DiI retrograde tract-tracing study. *Neuroscience Letters, 69*, 163–166.

Berridge, M. J. (1998). Neuronal calcium signaling. *Neuron, 21*, 13–26.

Bito, H. (1998). The role of calcium in activity-dependent neuronal gene regulation. *Cell Calcium, 23*, 143–150.

Canavier, C. C., Clark, J. W., & Byrne, J. H. (1991). Simulation of the bursting activity of neuron R15 in Aplysia: Role of ionic currents, calcium balance, and modulatory transmitters. *Journal of Neurophysiology, 66*, 2107–2124.

Chay, T. R. (1990). Electrical bursting and intracellular Ca^{2+} oscillations in excitable cell models. *Biological Cybernetics, 63*, 15–23.

Chay, T. R. (1996). Modeling slowly bursting neurons via calcium store and voltage-independent calcium current. *Neural Computation, 8*, 951–978.

Chay, T. R., & Keizer, J. (1983). Minimal model for membrane oscillations in the pancreatic beta-cell. *Biophysical Journal, 42*, 181–190.

Chay, T. R., & Rinzel, J. (1985). Bursting, beating, and chaos in an excitable membrane model. *Biophysical Journal, 47*, 357–366.

Goldbeter, A. (1996). Function of the rhythm of intercellular communication in *Dictyostelium*: Link with pulsatile hormone secretion. In A. Goldbeter (Ed.), *Biochemical oscillations and cellular rhythms* (pp. 345–347). Cambridge: Cambridge University Press.

Hodgkin, A. L., & Huxley, A. F. (1952). A quantitative description of membrane current and its application to conduction and excitation in nerve. *Journal of Physiology (London), 117*, 500–544.

Jenks, B. G., Buzzi, M., Dotman, C., Koning, K. H. De, Scheenen, W. J. J. M., Lieste, J. R., Leenders, H., Cruijsen, P., & Roubos, E. W. (1998). The significance of multiple inhibitory mechanisms converging on the melanotrope cell of *Xenopus Laevis*. *Annals New York Academy of Sciences, 839*, 229–234.

Koopman, W. J. H., Scheenen, W. J. J. M., Roubos, E. W., & Jenks, B. G. (1997). Kinetics of calcium steps underlying calcium oscillations in melanotrope cells of *Xenopus Laevis*. *Cell Calcium, 22*, 167–178.

Lieste, J. R., Koopman, W. J. H., Reynen, V. J., Scheenen, W. J. J. M., Jenks, B. G., & Roubos, E. W. (1998). Action currents generate stepwise intracellular Ca^{2+} patterns in a neuroendocrine cell. *Journal of Biological Chemistry, 273*, 25686–25694.

Loh, Y. P., & Gainer, H. (1977). Biosynthesis, processing and control of release of melanotropic peptides in the neurointermediate lobe of *Xenopus Laevis*. *Journal of General Physiology, 70*, 37–58.

Maruthainar, K., Loh, Y. P., & Smyth, D. G. (1992). The processing of β-endorphin and α-melanotropin in the pars intermedia of *Xenopus Laevis* is influenced by background adaptation. *Endocrinology, 135*, 469–478.

Neher, E. (1998). Vesicle pools and Ca^{2+} microdomains: New tools for understanding their roles in neurotransmitter release. *Neuron, 20*, 389–399.

Nowycky, M. C., & Pinter, M. J. (1993). Time courses of calcium and calcium-bound buffers following calcium influx in a model cell. *Biophysical Journal, 64*, 77–91.

Pozzan, T., Rizzuto, R., Volpe, P., & Meldolesi, J. (1994). Molecular and cellular physiology of intracellular calcium stores. *Physiological Review, 74*, 595–636.

Reinhart, P. H., & Levitan, I. B. (1995). Kinase and phosphatase activities intimately associated with a reconstituted calcium-dependent potassium channel. *Journal of Neuroscience, 15*, 4572–4579.

Rinzel, J., & Ermentrout, B. (1998). Analysis of neural excitability and oscillations. In C. Koch & I. Segev (Eds.), *Methods in neuronal modeling* (pp. 251–291). Cambridge, MA: MIT Press.

Roubos, E. W. (1997). Background adaptation by *Xenopus Laevis*: A model for studying neuronal information processing in the pituitary pars intermedia. *Comparative Biochemistry and Physiology, 118A*, 533–550

Scheenen, W. J. J. M., Jenks, B. G., Roubos, E. W., & Willems, P. H. G. M. (1994). Spontaneous calcium oscillations in *Xenopus Laevis* melanotrope cells are mediated by Ω-conotoxin sensitive calcium channels. *Cell Calcium, 15*, 36–44.

Scheenen, W. J. J. M., Jenks, B. G., Willems, P. H. G. M., & Roubos E. W. (1994). Action of stimulatory and inhibitory α-MSH secretagogues on spontaneous calcium oscillations in melanotrope cells of *Xenopus Laevis*. *Pflügers Archiv, 427*, 244–251.

Scheenen, W. J. J. M., Jenks, B. G, van Dinter, R. J. A. M., & Roubos, E. W. (1996). Spatial and temporal aspects of Ca^{2+} oscillations in *Xenopus Laevis* melanotrope cells. *Cell Calcium, 19*, 219–227.

Shibuya, I., & Douglas, W. W. (1993). Spontaneous cytosolic calcium pulsing detected in *Xenopus* melanotrophs: Modulation by secreto-inhibitory and stimulants ligands. *Endocrinology, 132*, 2166–2175.

Stojilkovic, S. S., & Catt, K. J. (1992). Calcium oscillations in anterior pituitary cells. *Endocrine Reviews, 13*, 256–280.

Stojilkovic, S. S., Tomic, M., Kukuljan, M., & Catt K. J. (1994). Control of calcium spiking frequency in pituitary gonadotrophs by a single-pool cytoplasmic oscillator. *Molecular Pharmacology, 45*, 1013–1021.

Vergara, C., Latorre, R., Marrion, N. V., & Adelman, J. P. (1998). Calcium-activated potassium channels. *Current Opinion in Neurobiology, 8*, 321–329.

Wang, X., & Rinzel, J. (1995). Oscillatory and bursting properties of neurons. In M. A. Arbib (Ed.), *The handbook of brain theory and neural networks* (pp. 686–691). Cambridge, MA: MIT Press.

Received May 25, 1999; accepted May 2, 2000.